Electrophoretic deposition of poly(3-decylthiophene) onto gold-mounted cadmium selenide nanorods

José-Antonio Garate,[a)] Niall J. English[,a,b)] Ajay Singh,[c)] Kevin M. Ryan,[c)] Damian A. Mooney [a,b)] and J.M.D. MacElroy [a,b)]*

The SFI Strategic Research Cluster in Solar Energy Conversion

(a) UCD School of Chemical and Bioprocess Engineering, (b) Centre for Synthesis and Chemical Biology, University College Dublin, Belfield, Dublin 4, Ireland.

(c) Materials and Surface Science Institute, Department of Chemical and Environmental Sciences, University of Limerick, Limerick, Ireland.

* Corresponding Author: Email: niall.english@ucd.ie, Tel +353-1-7161646, Fax +353-1-7161177

ABSTRACT

Molecular mechanisms of electrophoretic deposition (EPD) of P3DT poly(3-decylthiophene) molecules onto vertically aligned cadmium selenide arrays have been studied using large-scale, non-equilibrium molecular dynamics (MD), in the absence and presence of static external electric fields. The field application and larger polymer charges accelerated EPD. Placement of multiple polymers at the same lateral displacement from the surface reduced average deposition times due to ‘crowding’, giving monolayer coverage. These findings were used to develop and validate Brownian dynamics simulations of multi-layer polymer EPD in scaled-up systems with larger inter-rod spacings, presenting a generalised picture in qualitative agreement with random sequential adsorption.

KEYWORDS

Molecular dynamics, gold surfaces, electric field, electrophoretic deposition, nanorod, cadmium selenide, P3HT, P3DT, light-conducting polymer, polymer-heterojunction solar cell

Introduction

In recent years, the development of organic optoelectronic devices has seen a rise in demand for conjugated polymers, especially for deployment in polymer-heterojunction solar cells; this interest is motivated due to their potential possible application in low-cost, flexible, large-area devices.[1,2] The power conversion efficiencies of bulk-heterojunction solar cells employing poly(3-hexylthiophene) (P3HT) as the donor have recently reached values of around 4–5% under standard solar conditions, with phenyl butyric acid methyl ester (PCBM)-type materials as the acceptor.[3,4] However, in order to improve conversion efficiencies, alternating, vertically aligned geometries of donor and acceptor phases, such as alternating nanorods, appear to constitute ideal structures for maximisation of carrier transport.[5] Similar devices using metal oxide electrodes and high-workfunction anodes (e.g., Ag and Au) have been developed recently to reduce oxidation problems in lower-workfunction cathodes and degradation of the indium tin oxide (ITO)–poly(ethylenedioxythiophene) (PEDOT) interface in conventional solar cells.[6,7] Although these structures are challenging to fabricate, Ryan *et al*. have made considerable progress in recent years via electrophoretic deposition (EPD) of nanocrystal and nanorod electrodes of differing charge from organic (toluene) solutions, to achieve a good degree of vertical nanorod alignment,[8,9] and also in the formation of nanorod assemblies in electric fields.[10-14] These advances have the distinct advantage of being solution-processable, rather than requiring vacuum techniques. Titov and Kral have also carried out a recent modelling study of the self-assembly of colloidal nanorod superlattice, using van der Waals and Coulombic coupling between dipolar nanorod and their substrates.[15] Recently, we have become interested in applying these techniques of electric field-directed assembly and EPD (in solution-processable organic solvents) towards the formation of P3HT-type conducting polymers on nanorod assemblies, or, more generally, nano-architectures, using both experimental and modelling approaches.

In the past decade, there has been increasing attention towards the electrophoretic behaviour of polymers, and on polymer-EPD, in particular. For instance, Dhand et al have studied experimentally the EPD of conducting polymer films on ITO surfaces,[16] while Bentram et al[17] and Foo and Pandey[18] have carried out computer simulations of polymer-EPD, and Ma et al have assessed the validity of colloidal theories vis-à-vis experimental data for polymer electrophoresis in solution.[19] However, the fundamental details of the EPD process of the polymers onto the essentially vertically aligned nanorod motifs remains to be understood and characterised to a greater extent in terms of mechanistic details at the atomistic level. In this respect, direct non-equilibrium molecular dynamics (MD) simulation of EPD has much to offer our current understanding of this process.

In this study, we have conducted large-scale MD simulation (on systems containing up to around half a million atoms) of varying numbers of differently-charged poly(3-decylthiophene), P3DT, onto arrays of vertically aligned cadmium selenide nanorods mounted on gold surfaces in both the absence and presence of externally applied static electric fields (notwithstanding the intrinsic electric field already present due to separation of charges; *vide infra*). Our goals are to study the variation of polymer deposition times with number of P3DT, their extent of dipolar (rotational) orientation vis-à-vis the electric field direction (whether intrinsic or external), and the influence of polymer charge and external field strength on the dynamics of the EPD process. We then use these findings to develop and validate Brownian dynamics simulations of multi-layer polymer EPD in scaled-up systems with larger inter-rod spacings, presenting a generalised picture in qualitative agreement with random sequential adsorption. To the best of our knowledge, this is the first report of an MD simulation of EPD onto nanorod arrays.

Model Construction

The Au(111) surface's polarisable potential was obtained from the GoIP atomistic force field.[20] The cadmium selenide (CdSe) inter-atomic energy function (Lennard-Jones) was taken from ref. 21; it is relevant to highlight the ionic nature of the CdSe rods, consisting of a negatively- (-1.18*e*) and positively- (+1.18*e*) charged ions, respectively. The poly(3-decylthiophene) (P3DT) monomers were modelled using a general-purpose force field for alkylthiophenes, oligomers and polymers.[22] Due to the total zero charge of the P3DT molecules, they were protonated at the sulphur atoms to obtain an overall positive charge (cf. Fig. 1A, blue hydrogen atoms). The OPLS[23] potential was applied to the toluene solvent molecules and chloride ions (employed to render the whole system electroneutral), with the chloride ions located and stable at the gold surface during MD.

Initially a smaller prototype periodic cell was built (cf. Fig. 2A), in which the *z*-direction was that of 'heterogeneity'. It consisted of an orthogonal Au(111) surface with dimensions of 82 x 82 x 19 Å and four (2 x 2) vertical, *x*-*y* plane-hexagonal, CdSe nanorods built from a wurtzite crystal structure, with a diameter of 12 Å and a height of 20 Å, placed above the gold surface (at 1.8 Å therefrom, in terms of center-of-atom separation); the (negatively-charged) selenide layer was at the top of the nanorods, and each rod was separated by 24 Å from their respective geometric central axes in the *x*- and *y*-directions. The rods were electroneutral and consisted of alternating layers of Cd and Se in the 001 direction (cf. Fig. 2A). Simulations with the (positively-charged) cadmium layer at the top led to the intrinsic electric field oriented in the opposite direction that would achieve polymer-EPD onto the nanorod arrays, and a much (unrealistically) stronger external electric field was then required to counter-act this to achieve polymer-EPD. Therefore, the only realistic geometry to probe polymer-EPD required the selenide layer on top, and these results will be discussed here.

A single P3DT molecule was localised at a 100 Å (in terms of center-of-mass, COM) 'upwards' from the top of the rods in the *z*-direction, and centered in the *x*-*y* plane of the simulation box. The system was solvated with a pre-equilibrated liquid toluene box of dimensions 82 x 82 x 180 Å that was placed just above the upper layer of the Au surface. In addition, chloride ions were added to render the whole system electroneutral. After relaxation by MD (*vide infra*), the final dimension was 82 x 82 x 200 Å, and the system comprised a total of 133,939 atoms. For more details, please see Fig. 2A. Although these rods are much smaller than those used experimentally,[8-14] which would typically be in the 6-8 nm diameter and roughly 30 nm length range, the inter-rod spacing and cross-sectional rod areas were chosen to conform in approximate proportional ratio to typical experimental dimensions and rod coverage per unit area.[9-14] It was desired to study EPD of polymers onto the rod arrays using direct MD, rather than in between the rods: experimentally, EPD between rods does rely on several parameters that are difficult to achieve, and, especially, control, such as removal of surfactant while retaining the architecture. For this reason, the inter-rod separations were set to 24 Å to ensure EPD would take place onto the rods, rather than in between, and the other dimensions taken in proportion to experimental surface area coverage and rod dimensions. In addition, a further size constraint is that the maximum number of atoms which could be simulated feasibly by direct MD was less than one million with available Blue Gene/P resources, thereby limiting severely the size range of the nanorods which could be simulated. However, we later relax this constraint of smaller inter-rod spacings when using MD-derived Brownian dynamics (BD) simulations to probe multi-layer polymer EPD between rods on scaled-up system sizes for longer simulation timescales, which would be otherwise computationally intractable via direct MD.

After some test analyses (cf. Fig. 2 and the discussion below), the prototype cell was scaled to a bigger system with 36 (6 x 6 *x*-*y* plane) CdSe nanorods (with equal dimensions as the prototype case) were

located above an orthogonal 183 x 183 x 19 Å Au (111) surface and separated by (the same) 24 Å from their respective geometric central axes in the *x*- and *y*-directions; please see Fig. 1. A pre-equilibrated liquid toluene box was added just over the top of the gold surface with dimensions of 183 x 183 x 180 Å. From this initial setup, four periodic cells were constructed with 1, 4, 8 and 16 P3DT molecules at a 100 Å from the top of the rods (in terms of polymer COM) in the *z*-direction. These systems contained a total of 490,117, 489,070, 487,724 and 531,326 atoms, respectively. All systems were built using the program VMDv1.87, following separate MD relaxation, if necessary.[24]

[insert Fig. 1 about here]

Simulation Details

All MD simulations were performed using the software NAMDv2.6.[25] The PME[26] method was used to treat full long-range electrostatics. A cut-off distance of 12 Å was applied to real-space Ewald interactions. An equal value was used for van der Waals interactions, using a smooth switching function applied thereto between 10 and 12 Å. A multiple time step scheme was used with 1 fs for bonded interactions, 2 fs for short-range non-bonded interactions, and 4 fs for the reciprocal-space electrostatics evaluation, using the r-RESPA method.[27] All production runs were simulated using coupling to an NVT reservoir, using Langevin dynamics with a set point of 298 K and a damping coefficient of 1 ps^{-1}.[28] The SHAKE[29] algorithm was applied to constrain bond lengths to all hydrogen atoms and the polarisable charges of the gold surface.

Prior to production runs, initial relaxation MD simulations of 4 ns were performed without any P3DT molecules. Subsequently, the P3DT molecule(s) were inserted, and after energetic minimization, a second run was carried out with a temperature rescaling scheme, increasing the temperature by 0.298 K

every 1 ps until reaching the desired temperature of 298 K. For all of the studied systems, the CdSe nanorods and the gold surface atoms (with the exception of the mobile polarisable charges) were kept fixed.

In the case of the prototype system, four test runs were performed using a P3DT total charge of +10*e*, +8*e*, +5*e* and +2*e*, respectively. In addition, two more simulations using the +8*e* system, were run under the influence of a static external electric field (*e*-field) applied with field intensities, *E*, of 0.0065 and 0.0195 V/Å in the -*z* directions. The electric field exerts a force over atomic partial charges *ia* defined by:

$$f_{ia} = E\, q_{ia} \qquad (1)$$

In terms of the larger systems, the chosen charge for the P3DT was +0.2*e*, and, therefore, four zero-field simulations were run for the single-, quad-, octo- and 16-P3DT systems (one for each). Accordingly, four additional simulations under the effects of a static electric field of 0.0195 V/Å were also carried out. Typical external electric field intensities in experiment are estimated to be of the order of 1 V/μm,[8-14] so the external fields here are necessarily some two orders of magnitude larger than experiment, in order to induce EPD within an amenable timescale for large-system (half-million-atom) MD (say, within 50 ns), but are relatively small in intensity in comparison to intrinsic electric fields in condensed aqueous phases, for instance (1.5-2.5 V/Å),[30] and to previous non-equilibrium MD of electrophoresis by the authors.[31,32] As will be shown below (cf. Figs. 1B and 4), the relatively low strengths of the 0.0065 and 0.0195 V/ Å external fields used in this study were minor in terms of effects (deposition times) in comparison to the 'intrinsic' electric fields induced by separation of the P3DT charge from the those of the negatively charged top layer of the nanorods (although the negative charges of the chlorides at the

gold surface led to formal electroneutrality, they did not interact to any appreciable extent with the polymers, as evidenced by negligible computed interaction forces).

Regardless of the periodic cell and simulation conditions, all runs were performed until adsorption onto the rods surface was achieved. This was confirmed by visual inspection (*e.g.*, see figures 1B and 1E), where a constant value of the P3DT COM *z*-coordinate versus time plot produces a zero-slope (cf. Figs. 2B, 2D, 3A, 3B and the inserts of Fig. 4), and a sudden increase in van der Waals (vdW) *z*-direction interaction force between a P3DT molecule and the CdSe nanorods (cf. Figs. 2C and 3C) – indicating repulsion due to close contact, or 'docking'. Therefore, for the prototype systems, simulations lasted from 2 to 10 ns, saving coordinates every 1 ps, whilst simulations were of 16 to 24 ns for the larger systems, saving coordinates every 2 ps.

Results and Discussion

Prototype-system simulations

We performed simulations of the prototype periodic cells, with the aim of obtaining a more detailed description of the underlying mechanisms of EPD and to calibrate the aims of study for the larger systems. In Fig. 2, the results of these simulations are presented for the prototype case. Before discussing the results in more detail, it is important to remark that due to the configuration of the CdSe nanorods, in which the top Se layer is highly negatively charged, an intrinsic *e*-field emerges that will act in the *-z* – direction, affecting any charged species 'within its range' (see Fig. 2A and eq. 1); essentially, once the attractive Coulombic interaction (in the *z*-direction, due to the charge separation) overcomes local forces due to the solvent, the rate of attraction of the positively-charge polymer accelerates. In Fig. 2 B, we have shown the time-evolution of the *z*-coordinate of the P3DT COM for a +8*e*-charged molecule under the effects of the intrinsic *e*-field (in the zero-field case) and two external fields (*e*-field) of -0.0065 and

-0.0195 V/Å respectively, applied in the same direction (-*z*) as the intrinsic field. In all three cases, deposition is induced by the respective fields and, as expected, an increment in the field intensity reduces the time required for deposition. In Figs. 2C and 2D, the effect of different total P3DT charges was examined. In Fig. 3C, the *z*-component of the VdW and the electrostatic forces between the P3DT and the rods is depicted as a function of the distance between the *z*-coordinate of the P3DT COM, for various different charges. Accordingly, the higher the value of the charge, the larger the (absolute) value of the electrostatic force, and this exhibits an approximate $1/r^2$ variation with distance as the P3DT molecule gets closer to the topmost, negatively charge selenide layer of the nanorods, until contact is so close that repulsive (positive) vdW forces increase upon adsorption. Therefore, an interesting point to note is that the termination of the deposition process can be monitored depending on the VdW forces value. Likewise, the greater the charge, the less time is required for deposition (cf. Fig. 2D). From these observations, it is clear that the attractive electrostatics force dominates the EPD process, as expected. Given that we had observed clear effects of charge and field intensity in the prototype systems, we decided to carry out further analysis on larger, more realistic systems of EPD onto a 6 x 6 array of nanorods with a much more realistic overall P3DT charge of +0.2*e*.

Larger-system simulations

In addition to the study of deposition time, we gauged the extent of rotational alignment (due to dipolar coupling)[30] with the field (either intrinsic, or in addition to the external field) for each system (1-, 4-, 8- and 16-P3DT) throughout the simulations. This was done by consideration of the time-evolution of the angle vis-à-vis the (laboratory) *z*-axis made by the principal moment of inertia vector oriented along the P3DT axis (cf. Fig. 3 A & B – see the yellow arrow), labelled as Θ. As a representative example, the time-variation in the rotational alignment for the single-P3DT is shown in Fig. 3, for the zero (intrinsic)-

field and 0.0195 V/Å cases (although the full complexity of the deposition-time distributions is revealed for the multiple-P3DT case in Fig. 4); the angle, Θ, is perpendicular to the *z*-axis if it is 90°, or parallel when 0°. Initially, the polymer was placed perpendicular to the *z*-axis initially (at 100 Å COM-topmost rod distance), but a certain extent of alignment is clearly evident at about 30 Å distance, though more pronounced in the absence of the external field (where the alignment declines to some 5°). Following this, the adsorption, or docked, motif of the polymer is more energetically stable 'at close quarters' (once within 20 Å distance that relaxation of the vdW interactions becomes important – cf. Figs. 3 C & D), and this requires the P3DT to be oriented 'flat' (or in the *x*-*y* plane), with its principal moment inertia axis essentially in that plane (or again *de facto* perpendicular to the *z*-axis, i.e., Θ is about 70°). The faster deposition time of the P3DT in the external field results in less time for more pronounced rotational alignment (cf. Fig. 3 B), meaning that the maximal alignment occurs at around 25° at about 25 Å from the top of the nanorods. Such a trend of more limited rotational alignment, arising from dipolar coupling, due to faster translational motion has been observed previously for proteins in static electric and electromagnetic fields.[32]

Considering the deposition times, these are depicted for the quad-, octo-, and 16-P3DT systems in Fig. 4, and the average deposition times (with standard deviations) for all cases provided in Table I. It can be seen that the average deposition time is reduced by around 20% in each case in the presence of the external field. The average deposition time declines somewhat with increasing numbers of P3DT molecules (*e.g.*, from 20 to 16.5 ns from the single to 16-P3DT case, without the external field), although there is a broadening in the histogram as there is a 'crowding' effect with some molecules reaching the surface earlier for the 16-P3DT than in the single- or quad-polymer instances. Nonetheless, the surface coverage in the 16-P3DT case is such that there is still a monolayer of deposited polymers,

given that all molecules do adsorb on the surface (evident from the insets in Figs. 4 E & F and also the "bird's eye" view of Fig. 1 F.

Brownian Dynamics

To scale up the simulations to larger systems, so as to study multi-layer polymer-EPD between rods of larger spacing, we have employed a BD approach, in which the toluene solvent is removed to reduce the computational cost dramatically (adjusting electrostatic interactions appropriately with the relative dielectric constant of 2.4). Here, a Stokes' Law frictional force, $6\pi\mu a v_z(t)$, is applied to each polymer based on the characteristic projected surface-area-based radius in the z-direction, *a*. Stokes' Law was tested for its applicability for the applied field strengths in the earlier MD simulations by calculation of the Reynold's number (Re = $\rho va/\mu$),[32] and found to be less than 0.1 in all cases, indicating laminar-flow EPD and the applicability of Stokes' Law. For development and validation of BD simulations, it is necessary to infer the *de facto* dynamic viscosity experienced by the polymers in these systems from the direct MD results, checking for size dependence effects. Under laminar-flow conditions, the additional induced velocity by the external field is given by $qE/6\pi\mu a$, where *q* is the charge on the polymer and *E* the external field intensity.[32] By computation of the differences in zero- and in-field averaged EPD flow velocities over 0.5 ns intervals (based on *z*-distance traversed) and characteristic dimension *a* (based on the corresponding interval-averaged *z*-direction projected surface area-based radius), *e.g.*, from Figs. 2 and 3, one may infer effective viscosities of 0.55-0.75 $mNsm^{-2}$ from both the prototype and larger systems (exhibiting no particular size dependence), in good agreement with other OPLS[33] (0.65 $mNsm^{-2}$) and experimental[34] (0.55 $mNsm^{-2}$) estimates of toluene viscosity at 298 K.

Following good agreement of essentially identical BD simulations with direct MD (with μ as 0.65 $mNsm^{-2}$), scale-up to larger systems were undertaken to study inter-rod penetration for larger spacings.

The same polymer charge state of +0.2*e* was used for EPD on gold surfaces of roughly 1000 x 1000 Å in cross-section with varying (larger) number of rods, using larger inter-rod spacings of 40, 60 and 80 Å. 1000 polymers were placed approximately 100 Å distant from the top of the rods with total *z*-box dimension of around 200 Å, corresponding to double the largest previous concentration per unit surface area for the largest (16-polymer) direct-MD system, to allow for multi-layer deposition. External field strengths of 0.001, 0.0065, 0.0195 and 0.03 V/Å were applied, as well as the zero-field case, and findings averaged over three independent simulations.

The probability distributions of the radius of gyration and end-to-end distance of the first deposited layer are depicted in Fig. 5 as a function of inter-rod spacing; there was not found to be a substantial variation in these quantities depending on external field conditions, or in rotational alignment upon deposition. In the case of the 40 Å spacing, there is limited inter-rod penetration by the first deposited layer (with COM *z*-coordinates roughly at the top of the rods, as opposed to some 10 Å above for 24 Å spacing), but with substantial contraction in the end-to-end distance vis-à-vis larger spacings where there is more scope to extend somewhat along the surface (and for deeper penetration between rods, with COM z-coordinates up to 10 Å below the top of the rods).

[insert Fig. 5 about here]

The multi-layer polymer film growth vis-à-vis the *z*-coordinate of the rod-tops is shown in Fig. 6 for the 40 and 80 Å spacings until all polymers have deposited; the 0.001 V/ Å results were very similar to the zero-field case. The greater inter-rod penetration is clear in the 80 Å spacing, with partial penetration for the 40 Å case, along with more rapid deposition in larger external fields. The greater final film thicknesses in external fields mirror the greater extent of rotational alignment beyond the first

monolayer, where there is not a large energetic preference for gold-polymer adsorption. The growth in the film thickness appears to follow the general qualitative trend of a square root in time, characteristic of random sequential adsorption models onto two-dimensional surfaces.[35,36]

[insert Fig. 6 about here]

Conclusions

The molecular mechanisms of EPD of P3DT polymers onto vertically aligned cadmium selenide arrays have been studied using non-equilibrium MD, in the absence and presence of static external electric fields, and the variation in terms of system size (in the *x*-*y* plane, or the extent of the nanorod array), polymer charge, external field strength and number of polymer molecules studied. It was found that the 0.0195 V/Å field led to a roughly 20% decline in deposition times, while the maximal extent of rotational alignment with the field declined somewhat in the case of the external field, due to faster deposition. A larger polymer charge and bigger external field intensity also led to accelerated EPD. It was observed that a greater number of polymers led to a decline in the average deposition time due to a 'crowding' effect, although the number and initial lateral placement of the polymers at identical distance from the top of the nanorods led to monolayer coverage. The development of BD simulations parameterised for friction from direct non-equilibrium MD led to the study of multi-layer polymer EPD in larger systems with bigger inter-rod spacings. Greater distortion of the polymer occurred in the first monolayer for the 40 Å spacing, while the growth of film thickness was found to resemble the general physical picture of random sequential adsorption.

This study has highlighted the mechanisms of charged-polymer EPD on nanorod array as being dominated by electrostatic interactions, and has identified the external field intensity range (circa 0.01

V/Å) required to observe tangible effects within MD simulations, and remarked upon the delicate interplay between electro-induced translational and rotational motion. This study highlights the exciting prospects of large-scale MD and BD simulation in the future as a ‘design tool’ to optimise nanorod geometry and design for optimal polymer-heterojunction solar cell efficiency.

Acknowledgements

J.-A. Garate acknowledges useful interactions with researchers involved in the Science Foundation Ireland (SFI)-funded Solar Energy Conversion research cluster [Grant No. 07/SRC/B1160]. N.E. acknowledges useful discussions on with Kenneth Stanton and Kirill Igumenshchev. We thank SFI, HEANet, IBM and the Irish Centre for High-End Computing (ICHEC) for the provision of funds for and support of high-performance computing facilities (including Blue Gene/P). We also thank IBM and their staff at their Watson and Rochester computing centres for access to Blue Gene/P facilities (arranged via the Dublin Institute of Advanced Studies and ICHEC), together with support from the Blue Gene team at IBM’s Dublin offices.

REFERENCES

[1] G. Yu, J. Gao, J.C. Hummelen, F. Wudl, A.J. Heeger, Science 270 (1995) 1789.

[2] B.Y. Yu, A. Tsai, S.P Tsai, K.T. Wong, Y. Yang, C.W. Chu, , J.J. Shyue. Nanotechnology 19 (2008) 255202.

[3] L.M. Chen, Z. Hong, G. Li, Y. Yang, Adv. Mater. 21 (2009) 1434.

[4] G. Dennler, M.C. Scharber, C.J. Brabec, Adv. Mater. 21 (2009) 1323.

[5] H.S. Wang, L.H. Lin, S.Y. Chen, Y.L. Wang, K.H. Wei, Nanotechnology 20 (2009) 075201.

[6] Z. Xu, L.M. Chen, G. Yang, C.H. Huang, J. Hou, Y. Wu, G. Li, C.S. Hsu, Y. Yang, Adv. Funct. Mater, 19 (2009) 1227.

[7] H. Schmidt, H. Flügge, T. Winkler, T. Bülow, T. Ried, W. Kowalsky, Appl. Phys. Lett. 94, (2009) 243302.

[8] S. Ahmed and K. M. Ryan, Adv. Mat. 20 (2008) 4745.

[9] S. Ahmed and K. M. Ryan, Chem. Comm. 42 (2009) 6421.

[10] A. Singh, R.D. Gunning, A. Sanyal, K.M. Ryan, Chem Comm. 46 (2010) 7193.

[11] C. O'Sullivan, R.D. Gunning, C.A. Barrett, A. Singh, K.M. Ryan, J. Mat. Chem. 20 (2010) 7875.

[12] C. O'Sullivan, S. Ahmed, K. M. Ryan, J. Mat. Chem. 18 (2008) 5218.

[13] S. Ahmed, K. M. Ryan, Nano Letters 7 (2007) 2480.

[14] K. M. Ryan, A. Mastroianni, K. A. Stancil, H. Liu, A. P. Alivisatos, Nano Letters 6 (2006) 1479.

[15] A.V. Titov, P. Král, Nano Letters 8 (2008) 3605.

[16] C. Dhand, S.P. Singh, S.K. Arya, M. Datta and B.D. Malhotra, Anal. Chim. Acta 602 (2007) 244.

[17] F.W. Bentrem, R.B. Pandey and F. Family, Phys. Rev. E 62 (2000) 914.

[18] G.M. Foo and R.B. Pandey, Biomacromol. 1 (2000) 407.

[19] J. Ma, C. Wang and C.H. Liang, Mat. Sci. Eng. C 27 (2007) 886.

[20] F. Iori, R. Di Felice, E. Molinari, J. Comp. Chem 30 (2008) 1465.

[21] E. Rabani J. Chem. Phys. 116 (2002) 258.

[22] M. Moreno, M. Casalegno, G. Raos, S.V. Meille, R. Po, J. Phys. Chem. B 114 (2010) 1591.

[23] W.L. Jorgensen, J. Tirado-Rives J. Am. Chem Soc 110 (1988) 1657.

[24] W. Humphrey, A. Dalke, K. Schulten J. Mol.Graph. 14 (1996), 33.

[25] J. C. Phillips, R. Braun, W.Wang, J. Gumbart, E.; Tajkhorshid, E. Villa, C. Chipot, R. D. Skeel, L. Kal, K. Schulten J. Comput. Chem. 26 (2005) 1781.

[26] T. Darden, D.York, L. P. Pedersen, J. Chem. Phys. 98 (1993) 10089.

[27] M. Tuckerman, B. J. Berne, G. J. Martyna J. Chem. Phys. 97 (1992) 1990.

[28] G. S. Grest, K. Kremer, Phys Rev A, 33 (1986) 3628.

[29] J. Ryckaert, G. Ciccotti, H. Berendsen, J. Comp. Phys. 23 (1977) 327.

[30] N.J. English, J.M.D. MacElroy, J. Chem. Phys. 119 (2003) 11806.

[31] N.J. English, W.F. Long, Physica A, 388 (2009) 4091.

[32] N.J. English, G.Y. Solomentsev, P. O'Brien, J. Chem. Phys. 131 (2009) 035106.

[33] L. Zhao, T. Cheng, H. Sun, J. Chem. Phys. 129 (2008) 144501.

[34] B.A. Younglove, H.J.M. Hanley, J. Phys. Chem. Ref. Data 15 (1986) 1323.

[35] R Erban, S.J. Chapman, Phys. Rev. E, 75 (2007) 041116.

[36] E. Eisenberg, A. Baram, Europhys. Lett., 44 (1998) 168.

Table I: Average Polymer Deposition Times (cf. Fig. 4).

Number of P3DT Molecules	Deposition time (ns)	
	zero-field	e-field (-0.0195 V/Å)
1	19.98	14.87
4	15.54 ± 2.57	12.35 ± 0.76
8	16.38 ± 2.56	14.10 ± 2.24
16	16.5 ± 4.68	13.22 ± 1.70

Figure Captions

Figure 1: (A) Poly(3-decylthiophene) (P3DT) molecule protonated on the sulphur atom (blue hydrogen atoms). (B and E) Side views of the simulated periodic cells for the single- and 16-P3DT systems, respectively, with the positions of the P3DT(s) at different simulated times. Gold surface atoms are depicted in yellow, whilst (negatively charged) Se atoms are coloured red and (positively charged) Cd atoms are in blue. (C and F) Top view of the simulated periodic cells with deposited P3DT(s) for the single- and 16-P3DT(s) systems, respectively. (D and G) Side views of the complete simulated periodic cells (with the toluene solvent molecules included denoted in cyan) for the single- and 16-P3DT systems, respectively.

Figure 2: (A) Top, side and complete views of the prototype simulated periodic cells; the gold surface atoms are denoted in yellow, (negatively charged) Se atoms are coloured red, (positively charged) Cd atoms are shown in blue, while light blue shading is used for toluene solvent molecules. (B) *z*-coordinate of the P3DT centre-of-mass (COM) for the +8 prototype system versus simulation time for the zero-field case (black), -0.0065 V/Å field (grey) and -0.0195 V/Å condition (red). (C) *z*-direction force components acting on the P3DT from interaction with the rods: van der Waals (positive) and electrostatic (negative) cases versus the distance between the P3DT COM and the CdSe nanorods for the +10- (black), +8- (grey), +5- (blue), +2-(red) charged P3DT prototype systems. (D) *z*-coordinate of the P3DT COM versus simulation time for the +10- (black), +8- (gray), +5- (blue), +2- (red) charged P3DT prototype systems.

Figure 3: (A and B) Distance between the *z*-coordinate of the P3DT COM and the top of the CdSe nanorods (grey), the principal axis angle Θ vis-à-vis the *z*-axis, versus simulated time for the single-P3DT system for the zero-field and *e*-field (-0.0195 V/Å) cases. The insets depict graphical representation of the corresponding plots, with the yellow arrow indicating the direction of the principal axis vector. (C) VdW (grey) and electrostatic (black) polymer-rod interaction *z*-direction force components (on the polymer) versus the distance between the *z*-coordinate of the P3DT COM and the top of the CdSe nanorods. (D) z-direction electrostatic interaction force component on the polymer for the zero-field (black) and the -0.0195 V/Å *e*-field cases (grey) versus simulated time for the single-P3DT system.

Figure 4: (A, C and E) Normalised histograms of the deposition times for the quad-, octo-, and 16-P3DT systems, respectively, under zero-field conditions. (B, D and F) Normalised histograms of the deposition times for the quad-, octo-, and 16-P3DT systems, respectively, in the -0.0195 V/Å *e*-field case. Each inset corresponds to the original plots from which the histograms were derived.

Figure 5: Normalised probability distributions of the radius of gyration and end-to-end distances of the first-deposited layer from zero-field BD simulations for 40-, 60-, and 80 Å inter-rod spacings.

Figure 6: *x*-*y* plane-averaged *z*-position of the COM's of the uppermost-deposited polymers vis-à-vis the *z*-coordinate of the tops of the rods for the 40 and 80 Å spacings under zero-, 0.0195, and 0.03 V/Å fields.

Figure 1

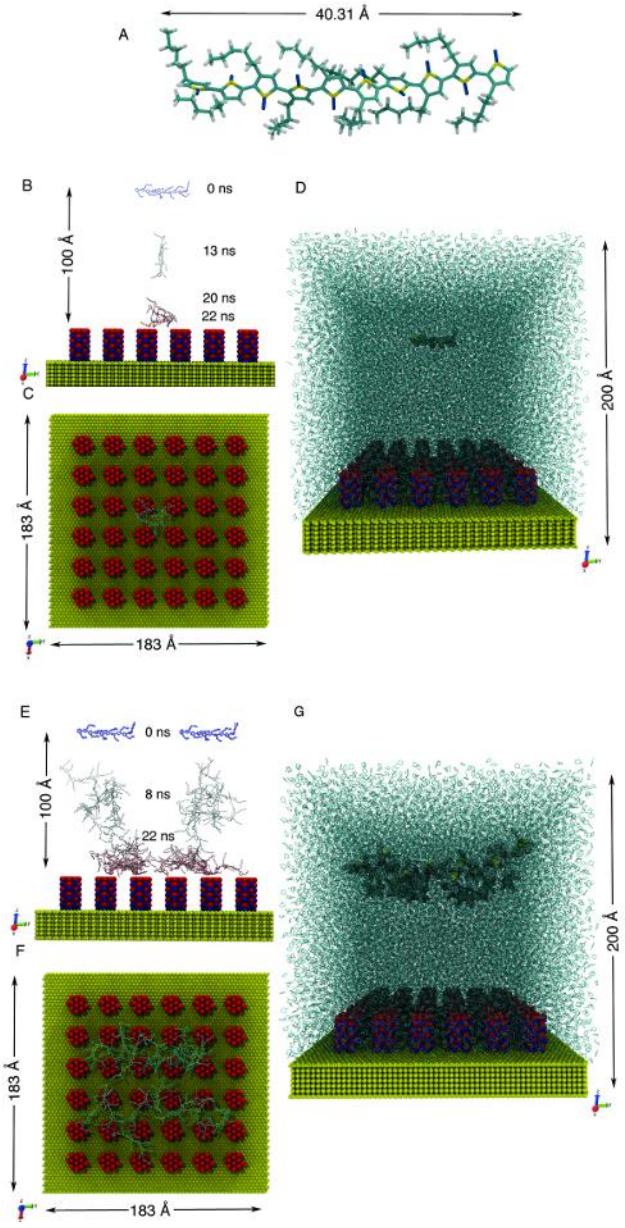
A
40.31 Å
B
0 ns
13 ns
20 ns
22 ns
100 Å
C
183 Å
183 Å
D
200 Å
E
0 ns
8 ns
22 ns
100 Å
F
183 Å
183 Å
G
200 Å

Figure 2

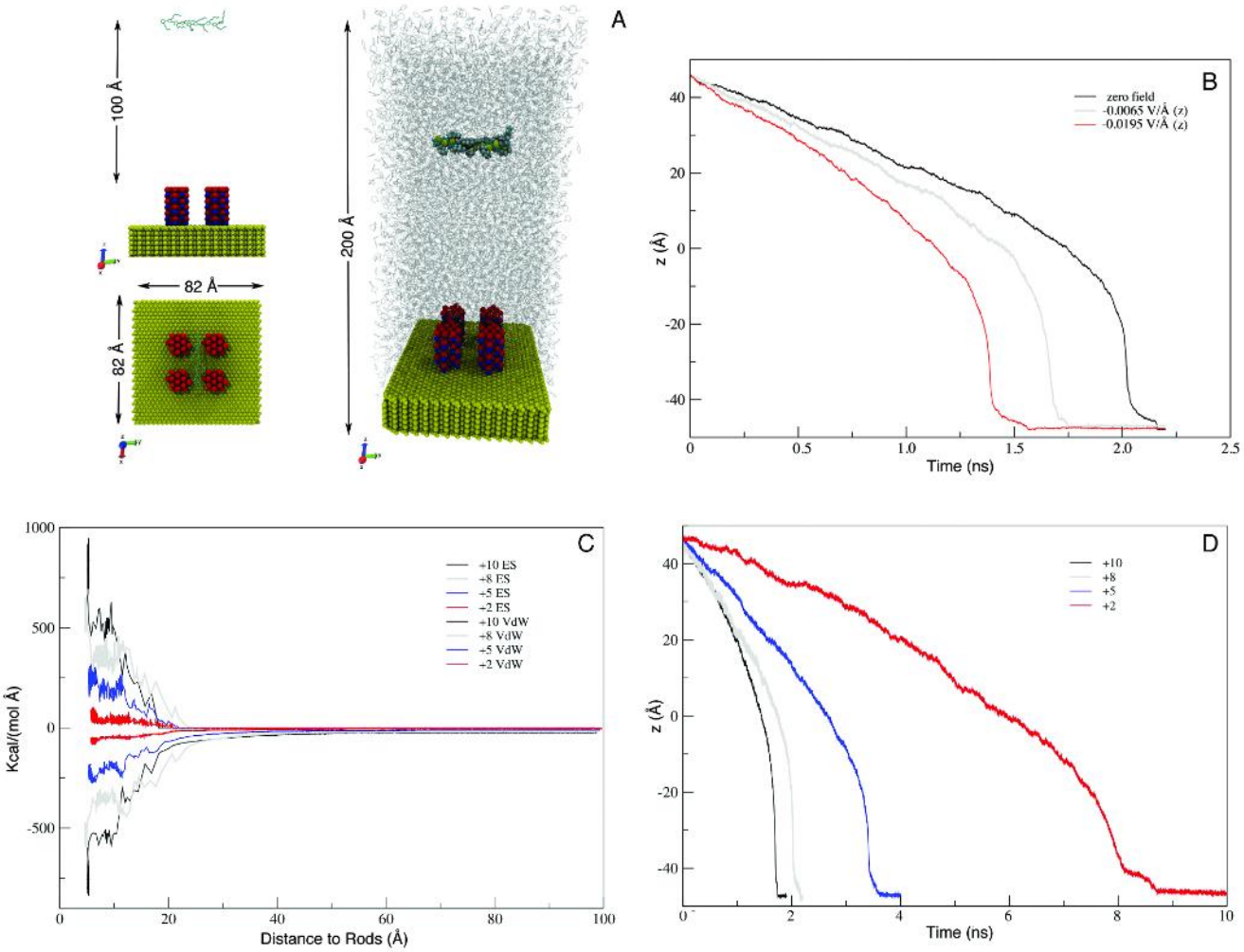
A
100 Å
82 Å
82 Å
200 Å
B
zero field
-0.0065 V/Å (z)
-0.0195 V/Å (z)
z (Å)
Time (ns)
C
+10 ES
+8 ES
+5 ES
+2 ES
+10 VdW
+8 VdW
+5 VdW
+2 VdW
Kcal/(mol Å)
Distance to Rods (Å)
D
+10
+8
+5
+2
z (Å)
Time (ns)

Figure 3

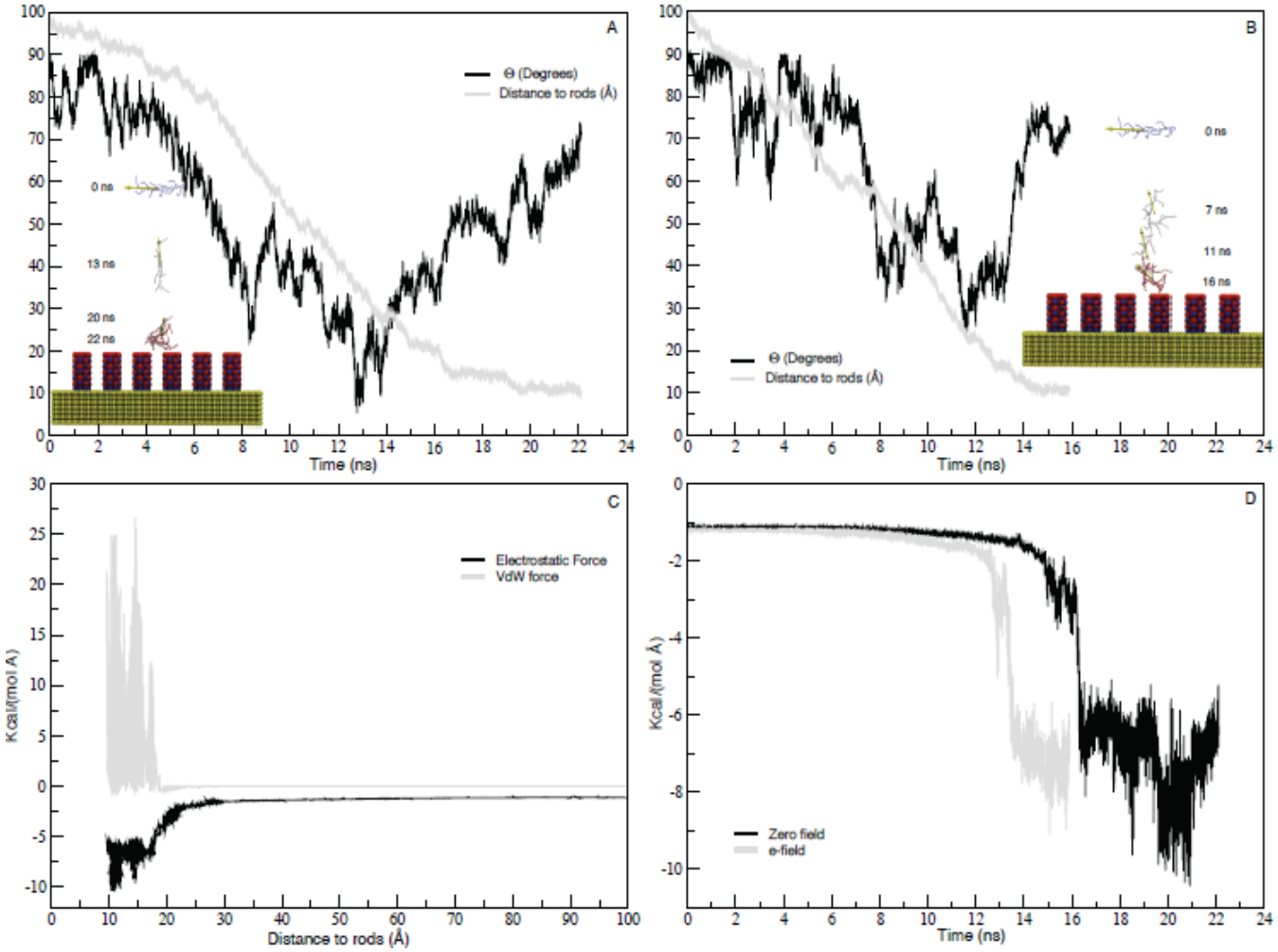
A
Θ (Degrees)
Distance to rods (Å)
0 ns
13 ns
20 ns
22 ns
Time (ns)
B
Θ (Degrees)
Distance to rods (Å)
0 ns
7 ns
11 ns
16 ns
Time (ns)
C
Electrostatic Force
VdW force
Kcal/(mol Å)
Distance to rods (Å)
D
Zero field
e-field
Kcal/(mol Å)
Time (ns)

Figure 4

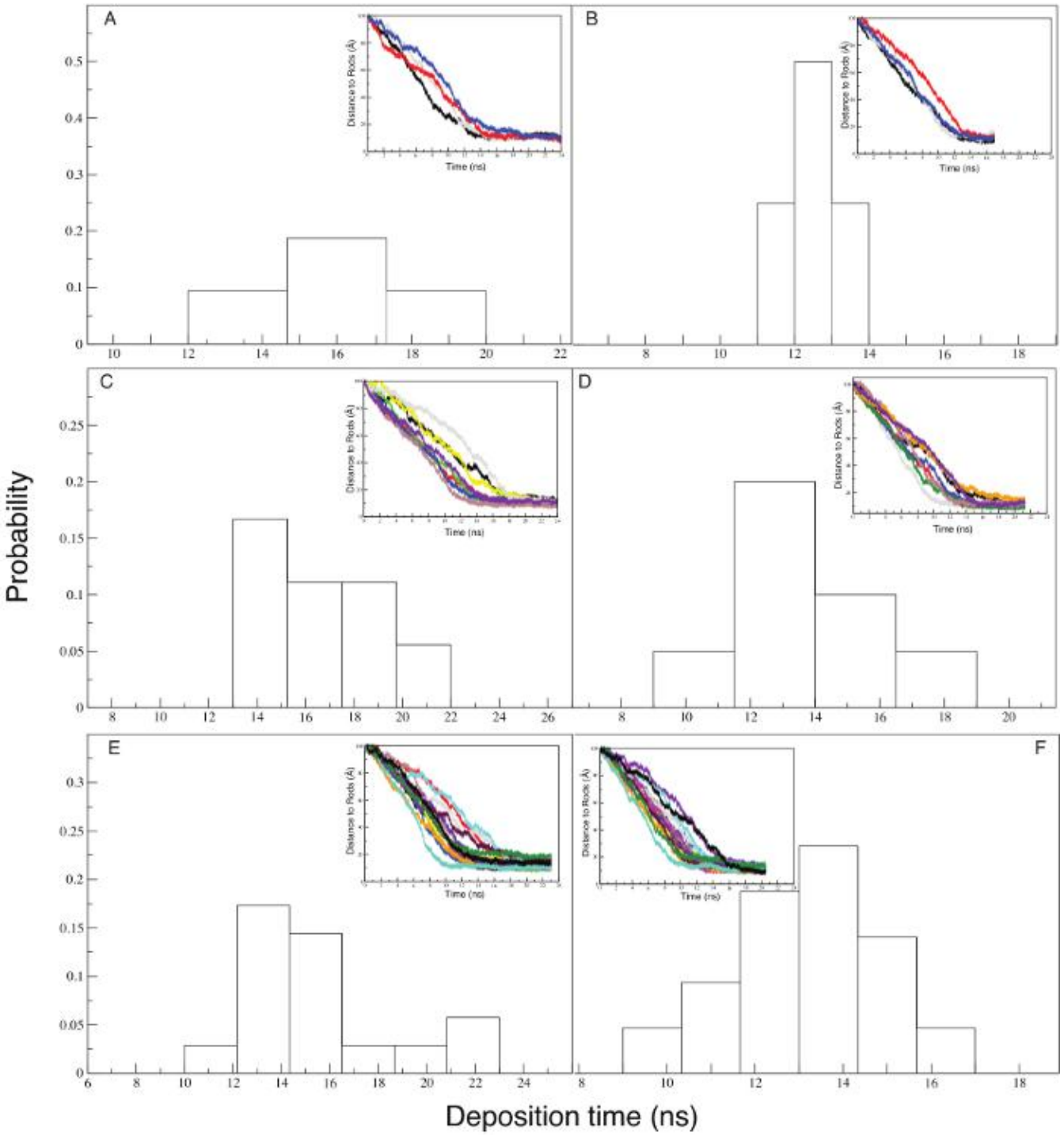
A
B
C
D
E
F
Probability
Deposition time (ns)
Distance to Rods (Å)
Time (ns)

Figure 5

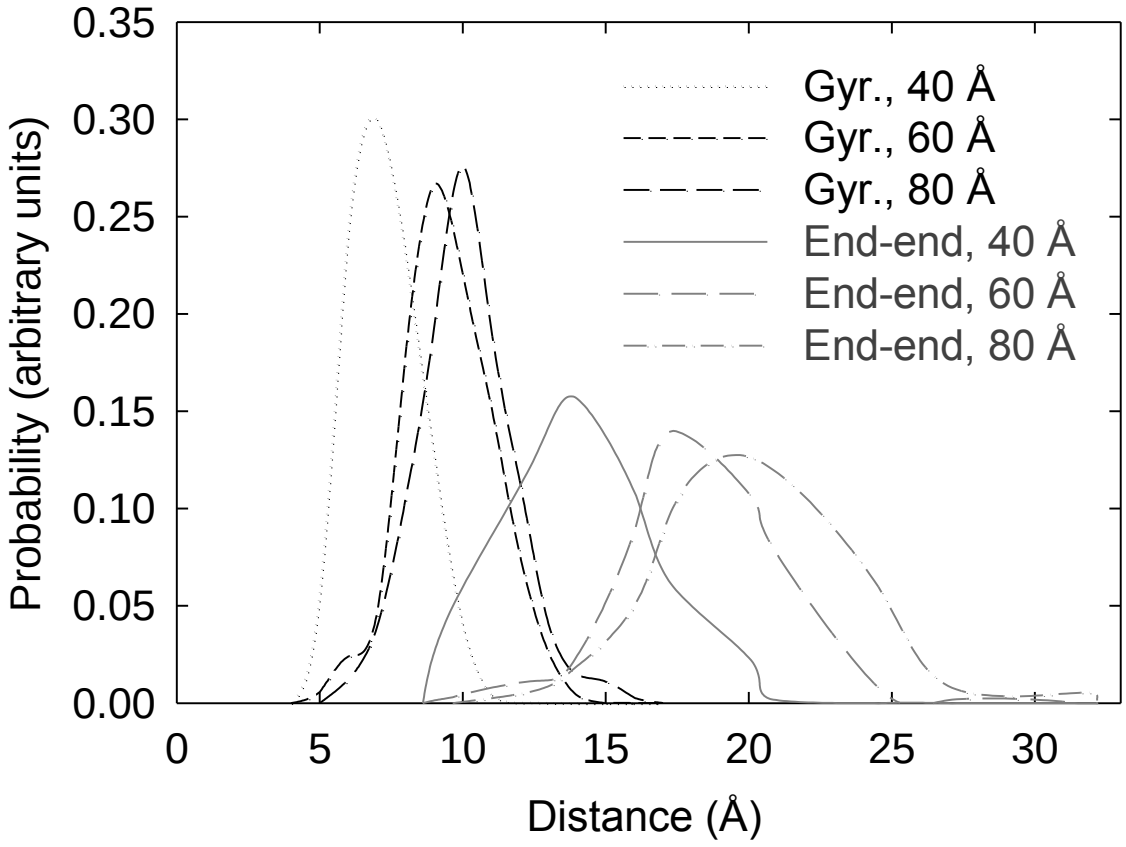
Probability (arbitrary units)
0.35
0.30
0.25
0.20
0.15
0.10
0.05
0.00
0
5
10
15
20
25
30
Distance (Å)
Gyr., 40 Å
Gyr., 60 Å
Gyr., 80 Å
End-end, 40 Å
End-end, 60 Å
End-end, 80 Å

Figure 6

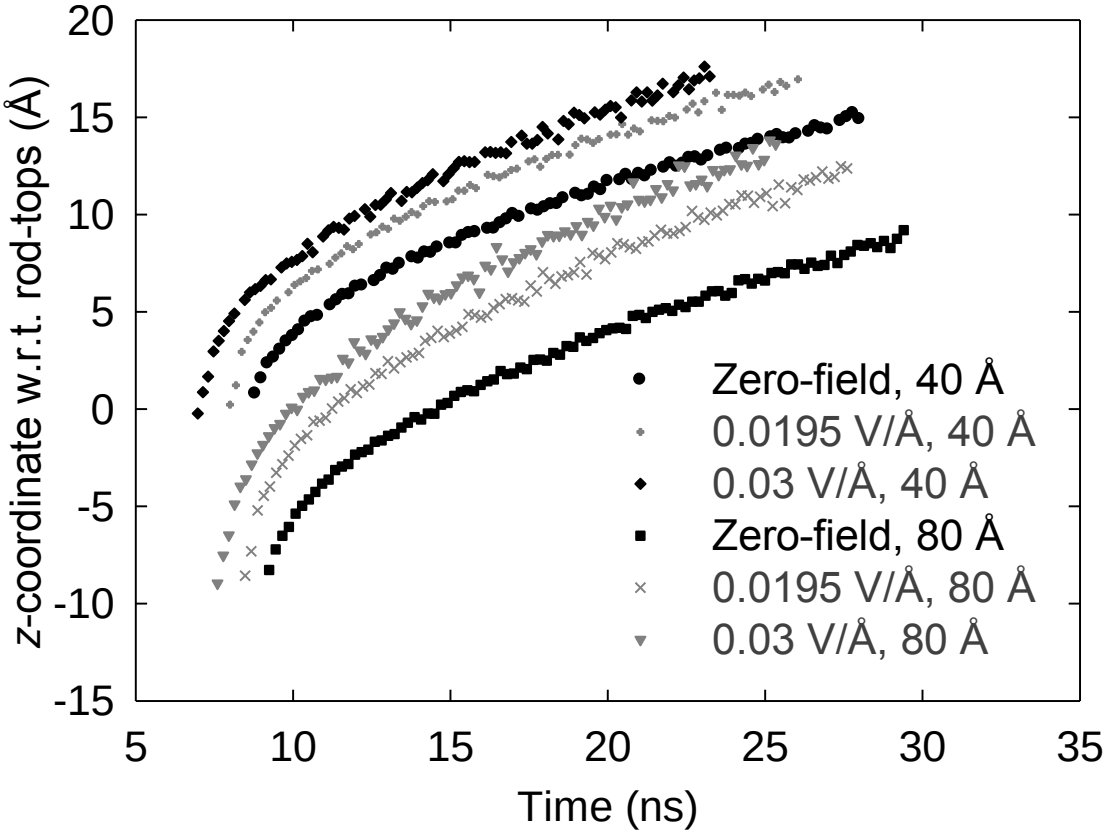
z-coordinate w.r.t. rod-tops (Å)
Time (ns)
Zero-field, 40 Å
0.0195 V/Å, 40 Å
0.03 V/Å, 40 Å
Zero-field, 80 Å
0.0195 V/Å, 80 Å
0.03 V/Å, 80 Å